References

[1] Wadleigh, K. H. et al, "Spinning Vehicle Nutation Damper," *Journal of Spacecraft and Rockets*, Vol. 1, No. 6, Nov.–Dec. 1964, pp. 588–592.

[2] Alper, J. R., "Analysis of Pendulum Damper for Satellite Wobble Damping," *Journal of Spacecraft and Rockets*, Vol. 2, No. 1, Jan.–Feb. 1965, pp. 50–54.

[3] Austin, F. and Zetkov, G. A., "Zero Mass-Shift Passive Damper for the Reduction of Precession in a Rotating Space Vehicle," *Journal of the Astronautical Sciences*, Vol. XVI, No. 1, Jan.–Feb. 1969, pp. 1–7.

[4] Cloutier, G. J., "Nutation Damper Design Principles for Dual-Spin Spacecraft," *Journal of the Astronautical Sciences*, Vol. XVI, No. 2, March–April 1969, pp. 79–87.

[5] Thomson, W. T. and Reiter, G. S., "Attitude Drift of Space Vehicles," *Journal of the Astronautical Sciences*, Vol. VII, No. 2, Summer 1960, pp. 29–34.

[6] Meirovitch, L. and Nelson, H. D., "On the High-Spin Motion Satellite Containing Elastic Parts," *Journal of Spacecraft and Rockets*, Vol. 3, No. 11, Nov. 1966, pp. 1597–1602.

Motion of Bubbles in a Rotating Container

IVAN CATTON*
University of California, Los Angeles, Calif.
AND
S. H. SCHWARTZ†
West Virginia University, Morgantown, West Va.

Nomenclature

a = acceleration
A_B = cross-sectional area of bubble
C_D = coefficient of drag
D = bubble diameter
g = gravitational constant
g_e = gravitational constant on the Earth
F_D = drag force
m = mass of liquid displaced by bubble
m_e = inertial mass
Re = Reynolds number
v = bubble velocity
V_B = bubble volume
$\dot{x}$ = velocity component in x direction
$\dot{z}$ = velocity component in z direction
ν = kinematic viscosity
ρ_l = liquid density
ρ_v = vapor density
$\Delta\rho = (\rho_l - \rho_v)$
σ = surface tension
θ = angle
ω = angular rotation

Introduction

THE basic goal is to examine the effect of the Coriolis force on the motion of bubbles after reaching steady state in a rotating system. The motion of bubbles, without rotation, will be in the opposite direction of the gravity vector. However, acceleration induced by artificially rotating the tank or due to the rotation about its own axis as it orbits the Earth, will cause the bubbles to travel in a direction at some angle with respect to the gravity vector. This will increase the time it takes a bubble to rise to the surface which may affect the liquid level rise in a low-gravity venting condition. In addition, the lateral motion of the bubbles away from the heated tank walls into the center portion of a tank may play a role in reducing thermal stratification.

Received October 22, 1971; revision received January 19, 1972.
Index categories: Multiphase Flows; Hydrodynamics.

* Assistant Professor of Engineering and Applied Science. Member AIAA.

† Associate Professor of Engineering.

Basic Equations

In writing the equations of motion for a bubble in a rotating system, an effective force on the bubble due to Coriolis accelerations must be considered. This, when added to the usual buoyancy force results in a bubble trajectory which can be significantly different from the case without rotation. The motion of the bubble will be taken to be two dimensional in a plane perpendicular to the axis of rotation. The geometry, coordinate system, as well as a force balance are given in Fig. 1.

Using Newton's second law for motion of the bubble results in the following equations for the x and z directions:

$$m\ddot{z} = (\rho_l - \rho_v)V_B[g_z + \omega^2(R - z)] - \tfrac{1}{2}C_D\rho_l A_B\dot{z}(\dot{z}^2 + \dot{x}^2)^{1/2} - 2m_e\omega\dot{x} \quad (1)$$

$$m\ddot{x} = (\rho_l - \rho_v)V_B[g_x + \omega^2 x] - \tfrac{1}{2}C_D\rho_l A_B\dot{x}(\dot{z}^2 + \dot{x}^2)^{1/2} + 2m_e\omega\dot{z} \quad (2)$$

For a given bubble, an expression for C_D is needed. A plot of C_D as a function of Reynolds number is given in Fig. 2 and it can be seen that C_D is not a single valued function. For a first approximation, the curve is broken into three distinct regions termed the Stokes flow regime, the transition regime and the spherical-cap regime. The transition regime describes the ellipsoidal bubble region falling between the spherical bubble domain and the spherical cap domain as described by Haberman and Morton.[1]

With this approach, it is possible to approximate the critical Reynolds numbers Re_t and Re_s where a bubble enters the transition or spherical-cap regimes. This is done by finding the intersection of the portion of the curve in the transition

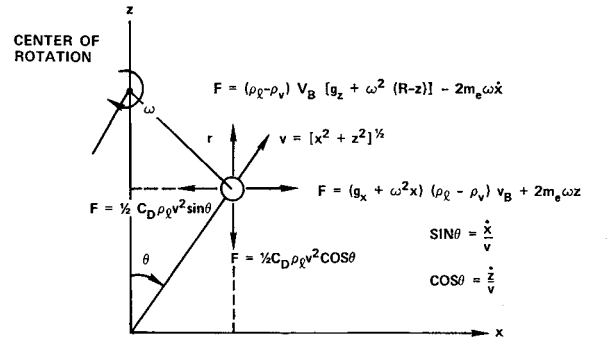

Fig. 1 Geometry, coordinate system and force balance on the bubble.

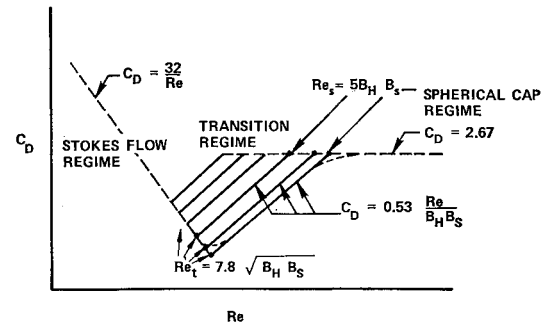

Fig. 2 Coefficient of drag vs Reynolds number.

regime with the curves in the Stokes and spherical-cap regimes, as shown in Fig. 1. The section of the curve in the transition regime is a function of the dimensionless parameter $(g\nu^4/\rho_l{}^3\sigma^3)$ while the other two portions remain fixed. Thus, the values of Re_t and Re_s will depend on this term. The expressions for these terms will be given below. The value of C_D in the Stokes flow regime is generally accepted to be equal to C_1/Re where the value of C_1 varies with the Reynolds number.[2] The upper and lower limits on C_D are 48 and 24. An approximate value of 32, lying half way between is used so that $C_D = 32/Re$. In the transition regime, the expression for the bubble velocity is generally written as

$$v = C_2(\Delta\rho g\sigma/\rho_l{}^2)^{1/4}$$

where Harmathy[3] reports a value of 1.53 for C_2, while Peebles and Garber[4] report 1.18. To the authors' knowledge, this discrepancy has not been resolved. This variation in reported results may be due to experimental differences or to the fact that $(g\Delta\rho\sigma/\rho_l{}^2)$ is not the proper parameter. In any event, it is necessary to be somewhat arbitrary in the selection of a value of C_2. The average of the two reported values, 1.36, will be used in this analysis.

The value of C_D in this region becomes

$$C_D = 0.53(g\rho_l{}^3D^4/\sigma^3)^{1/4}v$$

where it is assumed that $(\rho_l - \rho_v) \simeq \rho_l$. In the spherical-cap regime, the value of C_D is a constant and equal to approximately 2.67 as reported by Haberman and Morton. Here, the cross-sectional area of a bubble will deviate from $\pi D^2/4$ but the change will be neglected as a first approximation.

Since this analysis is concerned only with the steady-state regime, Eqs. (1) and (2) simplify to

$$(\dot{x}^2 + \dot{z}^2)^{1/2}\dot{z}\ 3C_D/4gD = 1 - \omega\dot{x}/g \tag{3}$$

$$(\dot{x}^2 + \dot{z}^2)^{1/2}\dot{x}\ 3C_D/4gD = \omega\dot{z}/g \tag{4}$$

when it is assumed that

$$g_z \gg \omega^2(R - z) \text{ or } R \gg z,\ g_x + \omega^2 x \ll \omega\dot{z}$$

and that the effective or inertial mass, m_e, can be written as $\frac{1}{2}(\rho_l - \rho_v)V_B$.

In the remaining development, distances are measured in units of bubble diameter, time in units of $(D/g)^{1/2}$ and velocity in units of $(gD)^{1/2}$. After making the equations dimensionless with this scaling, several parameters appear which will be represented by single letters for convenience. The following discussion will consider the bubble motion in each regime separately.

Stokes Regime

The solutions to Eqs. (3) and (4) describing the bubble motion in the Stokes flow regime written with the dimensionless parameters

$$A = (\omega^2D/g)^{1/2},\ B_s = (gD^3/\nu^2)^{1/2} \tag{5}$$

and

$$\dot{z} = \frac{1}{24}\left[\frac{B_s}{1 + (AB_s/24)^2}\right] \tag{6}$$

$$\dot{x} = (Ab_s/24)\dot{z} \tag{7}$$

The angle between the vertical and the trajectory which the bubble follows is $\tan^{-1}\theta = AB_s/24$ and the ratio of the velocity in the z direction with rotation to that without is

$$\dot{z}_\omega/\dot{z}_0 = 1/1 + (AB_s/24)^2 \tag{8}$$

The Stokes flow regime is valid as long as

$$Re = (\dot{z}^2 + \dot{x}^2)^{1/2}B_s < 7.8(\rho_l\sigma/g\mu^4)^{1/8} \tag{9}$$

Figure 3 demonstrates graphically the results obtained from Eqs. (6) and (7).

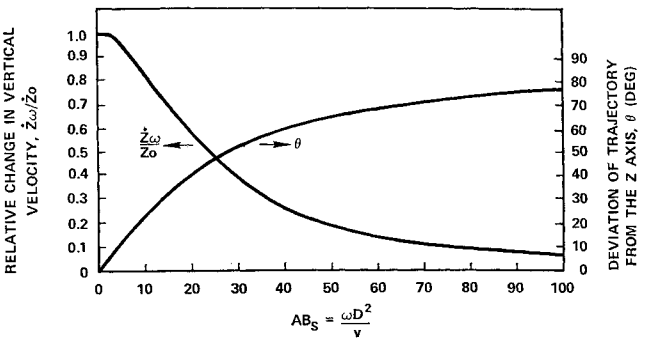

Fig. 3 Change in the vertical velocity and angular deviation for a bubble in the Stokes flow regime.

Transition Regime

In the transition regime, the equations describing the bubble trajectory are

$$(\dot{x}^2 + \dot{z}^2)\dot{z} = 2.514B_H(1 - A\dot{x}) \tag{10}$$

$$(\dot{x}^2 + \dot{z}^2)\dot{x} = 2.514B_HA\dot{z} \tag{11}$$

where $B_H = (\sigma^3/g^3\rho_l{}^3D^6)^{1/4}$. These equations are valid when

$$7.8(B_HB_s)^{1/2} = 7.8\left(\frac{\sigma^3}{\rho_l{}^3g\nu^4}\right)^{1/8} < \mathrm{Re} < 5\left(\frac{\sigma^3}{\rho_l{}^3g\nu^4}\right)^{1/4} = 5B_sB_H \tag{12}$$

Equations (10) and (11) were solved with a digital computing using the Newton-Raphson[6] method of solving equations. Results are illustrated in Figs. 4 and 5.

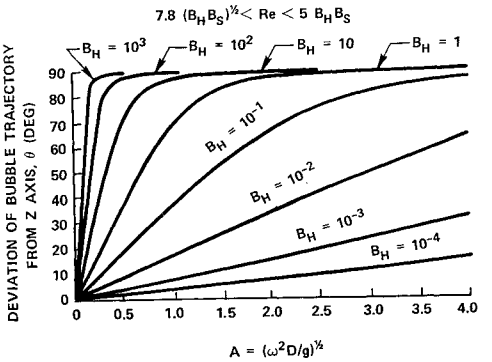

Fig. 4 Angular deviation of bubble trajectory in the transition regime.

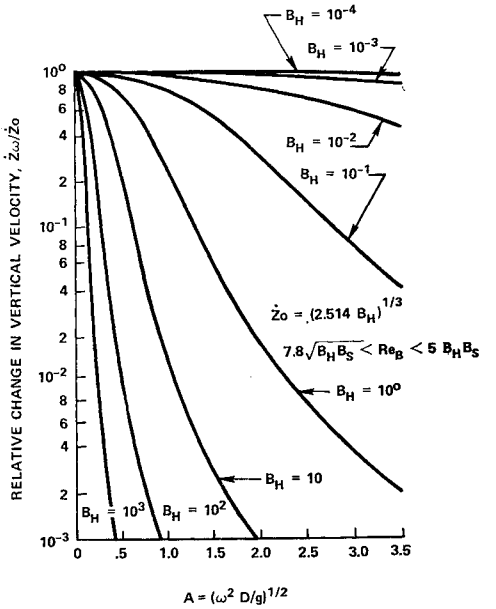

Fig. 5 Change in vertical velocity for a bubble in the transition regime.

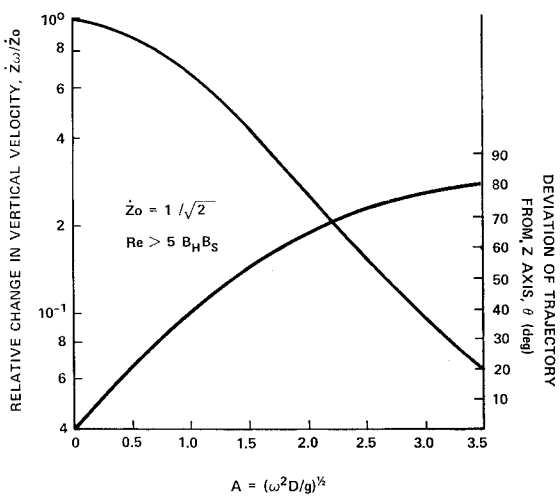

Fig. 6 Change in vertical velocity and angular deviation for a bubble in the spherical cap regime.

Spherical Cap Regime

When the velocities are large, the bubble will be in the last regime. This regime is called the spherical cap regime and the equations describing the terminal velocity of the bubble are

$$(\dot{x}^2 + \dot{z}^2)^{1/2}\dot{z} = \tfrac{1}{4}(1 - A\dot{x}) \tag{13}$$

$$(\dot{x}^2 + \dot{z}^2)^{1/2}\dot{x} = (A/4)\dot{z} \tag{14}$$

where the lower limit of applicability is

$$Re \geq 5(\sigma^3/\rho_l{}^3 g\nu^4)^{1/4} = 5B_H B_s$$

Figure 6 presents the results of Eqs. (13) and (14).

Discussion of Results

A cryogenic storage tank in a low-gravity environment is now selected as a specific example. Here the gravity level would be a function of the vehicle altitude, weight, and cross-sectional area. A range from 10^{-3} to 10^{-6} g/g_e is selected for illustration. Figure 7 shows the angular deviation from the z direction as a function of the bubble diameter for several gravity levels with liquid hydrogen.

Typical bubble sizes will depend on their origin. Although there will be a distribution of bubble breakoff diameters affected by these variables, a rough guideline provided by the Fritz[7] equation is used for purposes of comparison. The equation relates the breakoff diameter, D, to the gravitational constant where $D/D_{lge} \propto (g/g_e)^{-1/2}$. Values of D are shown in Fig. 8 for reference. For bubble diameters between 0.25 ft and the reference breakoff diameter of 2.5 ft at 10^{-6} g/g_e, the deviation from the vertical is approximately 35°. It can also be seen that bubbles smaller than 0.2 ft in diameter are in the

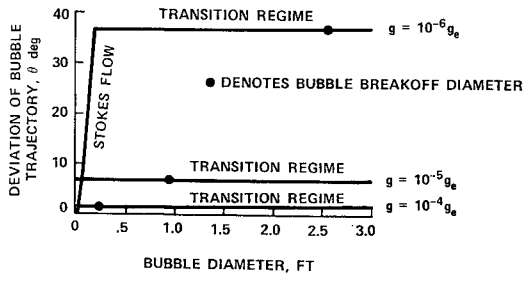

Fig. 7 Deviation of the trajectory of a bubble in liquid hydrogen from the longitudinal axis in an Earth oriented vehicle.

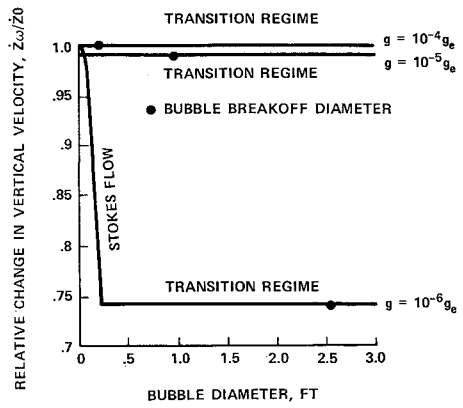

Fig. 8 Change in velocity of a bubble in liquid hydrogen in an Earth oriented vehicle.

Stokes regime and the deviation from the vertical is very sensitive to diameter.

One conclusion from these results is that bubbles 0.25 ft and larger, which originate below the surface at a distance greater than the tank diameter, will approach or reach the same area on one side of the tank before reaching the surface. This could have an effect on tank venting by increasing the local liquid entrainment caused by the vapor bubbles breaking through the surface on one portion of the surface.

In addition, the steady state velocity component in the vertical direction is also significantly reduced as shown in Fig. 8. For a bubble diameter of 2.5 ft, the terminal velocity in the z direction is reduced to 75% of its nonrotational value. The velocity reduction becomes very sensitive to gravity level when once the gravity level is below 10^5 g_e.

In a closed, heated container hot liquid rises to the surface and the subsequent evaporation results in a pressure rise. This problem arises in the storage of cryogenic propellants in space. For those values of heat flux where boiling may occur, the bubbles will leave the heated layer of liquid adjacent to the container walls and move through the center portion under the influence of the Coriolis force. If the liquid is subcooled, then these bubbles will tend to condense with the thermal energy being distributed in the subcooled bulk in the vicinity of the collapsing bubbles. Hence, this is a potential mode of energy transport which will tend to reduce the degree of stratification.

If the entire vehicle is artificially rotated to provide a larger gravitational field in space, the rotational speed ω is increased over that experienced when orbiting the Earth. As a result, it is expected that the above effects will be amplified for these cases. This is shown in Figs. 9 and 10 for liquid hydrogen.

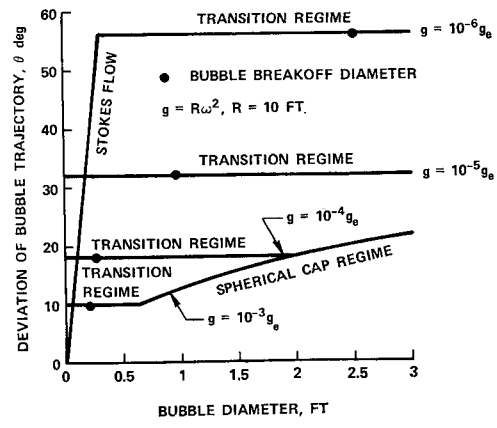

Fig. 9 Deviation of the trajectory of a bubble in liquid hydrogen from an axis through the center of rotation in a rotating laboratory.

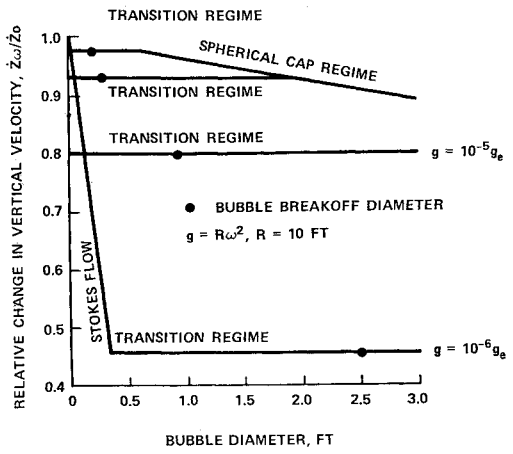

Fig. 10 Change in velocity of bubbles in liquid hydrogen towards the center of rotation in a rotating laboratory.

The rotational speed is expressed as $\omega = (a/R)^{1/2}$ where R is the distance measured from the center of rotation to the vicinity of the bubble. It is assumed here that R is essentially constant over the distance traveled by the bubble.

References

[1] Haberman, W. L. and Morton, R. K., "An Experimental Investigation of the Drag and Shape of Air Bubbles Rising in Various Liquids," Rept. 802, Sept. 1953. David Taylor Model Basin, Washington, D.C.

[2] Moore, D. W., "The Boundary Layer on a Spherical Gas Bubble," *Journal of Fluid Mechanics*, Vol. 16, 1963, p. 161.

[3] Harmathy, T. F., "Velocity of Large Drops and Bubbles in Media of Infinite or Restricted Extent," *AIChE Journal*, Vol. 6, 1960, p. 281.

[4] Peebles, F. N. and Garber, J. H., "Studies on the Motion of Gas Bubbles in Liquids," *Chemical Engineering Progress*, Vol. 49, 1953, p. 88.

[5] Milne-Thomson, L. M., *Theoretical Hydrodynamics*, 4th ed., Macmillan, New York, 1960.

[6] Scarborough, J. B., *Numerical Mathematical Analysis*, 5th ed., The John Hopkins Press, Baltimore, Md., 1962.

Effect of Nozzle Throat Radius of Curvature on Gasdynamic Laser Gain

JERRY L. WAGNER* AND JOHN D. ANDERSON JR.†
Naval Ordnance Laboratory, Silver Spring, Md.

RAPID supersonic, nonequilibrium expansions of hot, vibrationally excited CO_2—N_2—H_2O or He mixtures can produce population inversions and hence laser action in CO_2. This is the essence of the CO_2—N_2 gasdynamic laser. Interest in gasdynamic lasers is rapidly growing, and discussions in this regard can be found in Refs. 1–4, among others.

The heart of a typical gasdynamic laser is a bank of extremely short, minimum length contoured nozzles in which the N_2 vibrational energy is essentially frozen in the throat region. Such a sharp-cornered nozzle is sketched in Fig. 1a). Experimental and theoretical studies of the aerodynamic flow through such nozzles are described in Refs. 5 and 6. In particular, Greenberg et al.[5] clearly point out that the subsonic radius of curvature R_c (upstream of the sharp corner throat) should be made small, $R_c \approx h^*$, in order to enhance vibrational freezing and the subsequent laser gain.

This Note complements the study of Ref. 5 by examining the effect of extending the radius of curvature into the supersonic section, as sketched in Fig. 1b). By keeping the throat height constant and completely rounding the sharp corner, the nozzle of Fig. 1b) is easier to manufacture and align than the nozzle of Fig. 1a). However, this results in less vibrational freezing and hence reduced laser performance. The purpose of this Note is to indicate quantitatively the compromise in laser performance due to such rounding of the throat.

The present results were obtained from numerical experiments employing the time-dependent nonequilibrium nozzle flow analysis of Refs. 7 and 8. This analysis fully couples the vibrational kinetic rate equations with the governing quasi-one-dimensional flow equations of continuity, momentum and energy. Nonequilibrium conditions are included both upstream and downstream of the nozzle throat. A simplified vibrational model is used which approximates the detailed molecular energy transfer. The results of Refs. 9 and 10 show that the model and analysis of Ref. 7 yield reasonable agreement with experimental data for gasdynamic laser gain.

For the present investigation, the following conditions are assumed for gas mole fractions, area ratio, supply pressure, and supply temperature, respectively: $X_{CO_2} = 0.103$, $X_{N_2} = 0.885$, $X_{H_2O} = 0.012$, $A/A^* = 20.07$, $P_o = 10.2$ atm, and $T_o = 1600°K$. These are typical conditions for CO_2—N_2 gasdynamic lasers. The two-dimensional nozzle shape employs a linear subsonic contour with a 45° entrance angle, α, a prescribed radius of curvature at the nozzle throat, and a 37.5° initial supersonic expansion angle, θ, followed by a minimum length supersonic contour [see Fig. 1b)]. Results are obtained for throat heights, $h^* = 0.3$ mm, 1.0 mm, and 2.0 mm, with radii of curvature equal to 0, 1, 2, and 3 throat heights. Since the nozzles are geometrically similar, a decrease in throat height results in a corresponding decrease in nozzle length. Consequently, larger axial gradients (dp/dx, $d\rho/dx$, etc.) and therefore greater vibrational freezing occurs as the throat heights become smaller.

Typical gain profiles for $h^* = 1.0$ mm, 0.3 mm, and 2.0 mm

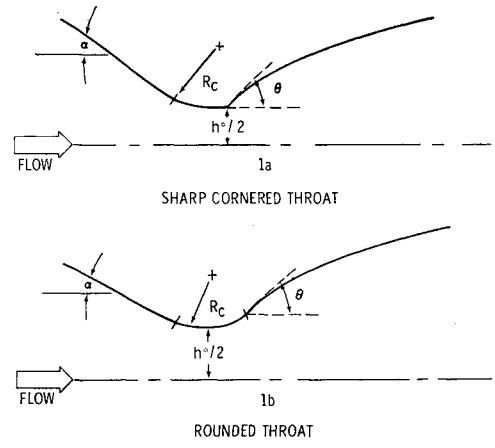

Fig. 1 Typical nozzle contours for gas dynamic lasers.

Received November 11, 1971; revision received February 14, 1972. Work supported by the Naval Ordnance Systems Command.

Index categories: Lasers; Nozzle and Channel Flow; Thermochemistry and Chemical Kinetics.

* Aerospace Engineer, Hypersonics Group, Aerophysics Division.

† Chief, Hypersonics Group, Aerophysics Division. Member AIAA.